COBEM 2021 26th International Congress of Mechanical Engineering
November 22-26, 2021, Virtual Congress, Brazil
ABCM Associação Brasileira de Engenharia e Ciências Mecânicas

COB-2021-1823
Influence of the heat transfer fluid on the performance of an active magnetic regenerator: a sensitivity analysis

Elias Pagnan
elias.pagnan@polo.ufsc.br
Guilherme Fidelis Peixer
guilherme.peixer@polo.ufsc.br
Higor Feltrin Teza
higor.teza@polo.ufsc.br
Bernardo Peressoni Vieira
bernardo.vieira@polo.ufsc.br
Jaime Andrés Lozano
jaime@polo.ufsc.br
Jader Riso Barbosa Jr
jrb@polo.ufsc.br

Polo - Research Laboratories for Emerging Technologies in Cooling and Thermophysics, Department of Mechanical Engineering Federal University of Santa Catarina, Florianópolis, SC, 88040-900, Brazil

Abstract. *Magnetic refrigeration presents itself as one of the most promising alternatives to vapor compression refrigeration due to potentially higher efficiencies and sustainability. This technology is based on the concept of the active magnetic regenerator (AMR), a storage-type heat exchanger subjected to alternating heat transfer fluid flow through a porous matrix formed by magnetocaloric material (MCM), which changes its temperature according to the magnetocaloric effect (MCE). The AMR performance has been studied by numerous works, however, the influence of the heat transfer fluid is usually left out or superficially analyzed. This way, the objective of the present work is to utilize an experimentally validated one-dimensional AMR model to numerically evaluate the AMR performance under the effect of varying some of the fluid thermohydraulic properties and using different existing fluids applied in thermal devices. The results for the fluid properties show that increasing the thermal conductivity has impressive impacts in the cooling capacity, furthermore, increasing the fluid density has great impacts in the pumping power and in reducing the viscous losses dominance with increasing mass flow rate. For the existing fluids, adding metallic nanoparticles to enhance water properties showed improved and promising results in terms of cooling capacity and coefficient of performance.*

Keywords: *magnetic refrigeration, active magnetic regenerator, numerical simulation, performance evaluation, heat transfer fluid*

1. INTRODUCTION

Refrigeration systems are fundamental technologies in today's world. Nowadays, vapor compression refrigeration is the most common principle applied in such systems, a mature technology that after more than a century of development dominates domestic and commercial refrigeration and air conditioning applications (Bansal *et al.*, 2012). Nevertheless, conventional mechanical compression systems still have inherent inefficiencies (Monfared, 2018) and operate with hazardous and environmentally harmful gases. Hence, alternatives are necessary to pursue higher energy efficiencies and not rely on volatile refrigerants.

Among these alternatives, magnetic refrigeration has been demonstrated as one of the leading contenders to be employed. Magnetic refrigeration relies on the reversible nature of the magnetocaloric effect (MCE), defined as the thermal response of a magnetic material when subjected to a varying magnetic field, with potential to be thermodynamically more efficient than conventional systems (Trevizoli, 2015). Additionally, it also operates with a solid-state refrigerant coupled with a sustainable heat transfer agent, avoiding the reliance on volatile refrigerants. Furthermore, one of the critical components, the magnet, can be reused or recycled.

The active magnetic regenerator (AMR) (Barclay and Steyert, 1982) is a storage-type heat exchanger subjected to alternating heat transfer fluid flow through a porous matrix formed by magnetocaloric material (MCM), which changes its temperature according to the MCE. The AMR can operate according to different themodynamic cycles, but the most common is the Brayton cycle (Trevizoli, 2015). An AMR based on the ideal thermo-magnetic Brayton cycle operates

with four steps (Rowe *et al.*, 2005). In real devices, however, an ideal AMR thermo-magnetic Brayton cycle is usually not possible. Hidraulic and magnetic system limitations give rise to fluid flow and magnetic profiles that impact the cycle (Fortkamp, 2019). Nevertheless, a schematic diagram is presented in Fig. 1 and the steps of the cycle are described below:

1. **Adiabatic magnetization:** the modulus of the aplied magnetic field is increased over the AMR adiabatically. Due to the MCE, the MCM temperature increases.
2. **Constant magnetic field cold blow:** the aplied magnetic field is kept constant and fluid from the cold reservoir flows through the porous magnetized MCM matrix, absorbing heat from the porous medium. As a consequence, the fluid temperature increases above the hot reservoir temperature and rejects heat to the latter.
3. **Adiabatic demagnetization:** the modulus of the aplied magnetic field is reduced to zero over the AMR adiabatically. Due to the MCE, the MCM temperature decreases.
4. **Constant zero magnetic field hot blow:** the aplied magnetic field is kept constant and fluid from the hot reservoir flows through the porous demagnetized MCM matrix, rejecting heat to the porous medium. As a consequence, the fluid has its temperature decreasesed below the cold reservoir temperature and absorbs heat from it (refrigerates it).

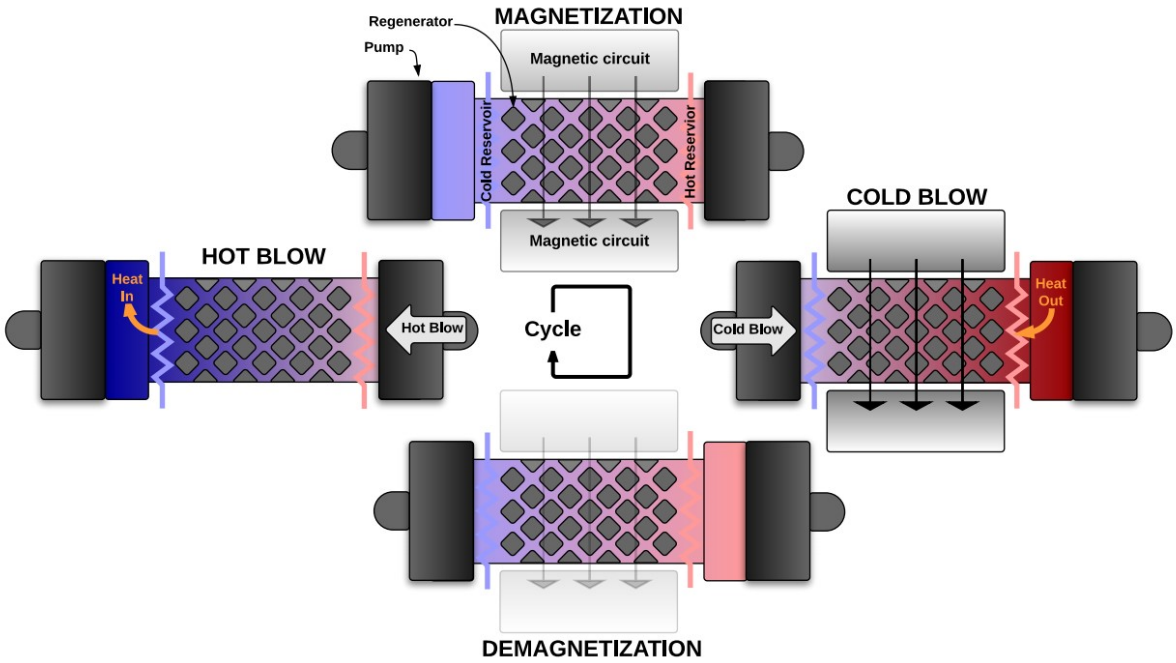

Figure 1: Schematic diagram of an AMR based on the ideal thermo-magnetic Brayton cycle (Trevizoli, 2015).

As presented above, it becomes evident that the heat transfer fluid plays a critical part in the cycle. The present work starts investigating the influence of heat transfer fluid properties on the AMR performance to identify which ones have the greater impact. For that, numerical simulations were conducted with an experimentally validated one-dimensional AMR model (Trevizoli *et al.*, 2016; Vieira, 2020). On the present work, variations on the following heat transfer fluid properties and related quantities were made: i) thermal conductivity; ii) density. Then, an analysis of the AMR performance operating with some existing heat transfer fluids (applied in thermal devices) is carried out.

For the purpose listed above, a regenerator geometry and operating parameters were defined and simulated with changes on the heat transfer fluid properties mentioned above, using water properties as reference. The baseline AMR operates with a 2 vol.% ENTEK water solution, which has essentially the same properties as pure water. The numerical results of the cases with changes on fluid properties were then compared in terms of cooling capacity ($\dot{Q}_{\mathrm{c}}$), coefficient of performance (COP_{AMR}) and pumping power ($\dot{W}_{\mathrm{pump}}$) with the results of an AMR using water as heat transfer fluid. The same comparison is carried out with the real world heat transfer fluids.

2. AMR MODEL

2.1 Governing equations

All simulations were performed with an an experimentally validated one-dimensional AMR model. The numerical model solves the momentum and energy equations on the fluid phase and the energy equation in the solid phase (MCM).

The equations are solved by the Finite Volume Method approach. The following assumptions are made: one-dimensional flow, low porosity medium, body forces absence, incompressible and laminar flow, fluid properties evaluated at a mean temperature. Only the governing equations mentioned above will be shown in the present work, but further information about the AMR model can be found at (Trevizoli *et al.*, 2016) and (Vieira, 2020).

The basic geometry of the model is shown in Fig. 2. The present work assumed regenerators to be adiabatic to the environment and the solid porous medium (MCM) composed of packed spheres. In the following equations, the indices "f" refers to the fluid phase and "s" to the solid phase. The momentum equation for the fluid phase, also known as Brinkman-Forcheimer equation (Kaviany, 1995), simplifies to:

$$\frac{\rho_\mathrm{f}}{\varepsilon}\left(\frac{\partial u}{\partial t}\right) = -\frac{\partial P}{\partial z} - \frac{\mu_\mathrm{f}}{K}u - \frac{c_\mathrm{E}\rho_\mathrm{f}}{K^{1/2}}|u|u \tag{1}$$

where ρ_f is the fluid density, ε is the porous medium porosity, u is the Darcy velocity, P is the pressure, μ_f the fluid dynamic viscosity, K is the permeability and c_E the Ergun constant (Ergun, 1952). The momentum equation returns the pressure drop along the regenerator.

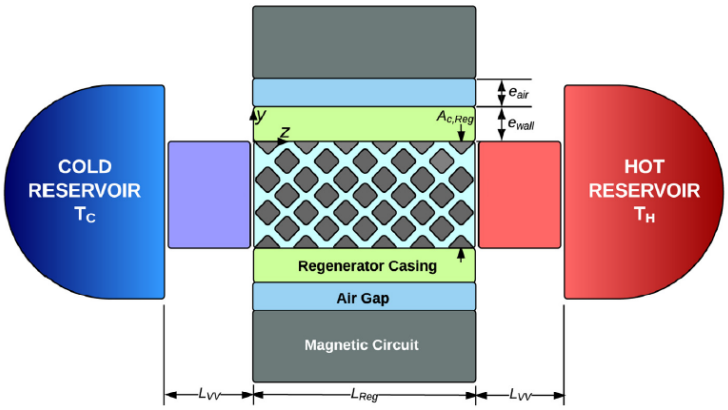

Figure 2: Geometry domain for the AMR numerical model (Trevizoli *et al.*, 2016).

The energy equation for the fluid phase is given by:

$$\rho_\mathrm{f}(T)c_{\mathrm{p,f}}(T)\left(\varepsilon\frac{\partial T_\mathrm{f}}{\partial t} + u\frac{\partial T_\mathrm{f}}{\partial z}\right) = h(z)\beta\left(T_\mathrm{s} - T_\mathrm{f}\right) + \left|u\frac{\partial P}{\partial z}\right| + \varepsilon\left[k_\mathrm{f}^\mathrm{eff} + \rho_\mathrm{f}(T)c_{\mathrm{p,f}}(T)D_\parallel\right]\frac{\partial^2 T_\mathrm{f}}{\partial z^2} + \dot{q}_\mathrm{csg} \tag{2}$$

where $c_{\mathrm{p,f}}$ is the fluid specific heat capacity, T_f is the fluid temperature, h is the interstitial heat transfer coefficient, β is the interstitial heat transfer area, T_s is the solid temperature, $k_\mathrm{f}^\mathrm{eff}$ is the fluid effective thermal conductivity, $D_\parallel$ is the dispersion coefficient and $\dot{q}_\mathrm{csg}$ is the casing heat transfer.

Finally, the energy equation for the solid phase is written as:

$$\rho_\mathrm{S}(T)c_\mathrm{S}(T)(1-\varepsilon)\frac{\partial T_\mathrm{S}}{\partial t} = h(z)\beta\left(T_\mathrm{f} - T_\mathrm{S}\right) + (1-\varepsilon)k_\mathrm{S}^\mathrm{eff}\frac{\partial^2 T_\mathrm{S}}{\partial z^2} + \dot{q}_\mathrm{MCE} \tag{3}$$

where ρ_s is the solid density, c_S is the solid specific heat capacity and $k_\mathrm{S}^\mathrm{eff}$ is the solid effective thermal conductivity. The heat source term $\dot{q}_\mathrm{MCE}$ represents the MCE, using the built-in approach. The solid (MCM) properties are calculated using measured data from the material. The AMR model uses input operating conditions to solve the governing equations during one full cycle. Boundary conditions, closure relations for the terms in the equations and convergence criteria are discussed in profund details in (Lang, 2018; Vieira, 2020).

2.2 Important parameters and relations

An important parameter for heat exchangers is the Number of Transfer Units (NTU), which represents the thermal size of the heat exchanger (AMR) and is given by:

$$NTU = \frac{hA_\mathrm{HT}}{\dot{m}_\mathrm{f}c_{p,\mathrm{f}}} \tag{4}$$

where A_HT represents the heat transfer area. The Reynolds number based on the particle diameter (Re_dp), the Prandtl number Pr, the Nusselt number based on the particle diamenter (Nu_dp) and the interstitial heat transfer coefficient (h) are given by:

$$Re_\mathrm{dp} = \frac{\rho_\mathrm{f}ud_\mathrm{p}}{\mu_\mathrm{f}} \tag{5}$$

$$Pr = \frac{c_{\mathrm{p,f}}\mu_{\mathrm{f}}}{k_{\mathrm{f}}} \tag{6}$$

$$Nu_{\mathrm{dp}} = \frac{hd_{\mathrm{P}}}{k_f} = 2\left(1 + \frac{4\,(1-\varepsilon)}{\varepsilon}\right) + (1-\varepsilon)^{1/2}\, Re_{\mathrm{dp}}^{0.6}\mathrm{Pr}^{1/3} \tag{7}$$

where d_{p} is the particle diameter. The Nusselt number (Eq. (7)) was calculated via the correlation developed by Pallares and Grau (2010) .

2.3 Performance metrics

After convergence is achieved in the AMR model, the following parameters are calculated taking the cycle average: cooling capacity ($\dot{Q}_{\mathrm{c}}$), rejected heat rate ($\dot{Q}_{\mathrm{h}}$), pumping power ($\dot{W}_{\mathrm{pump}}$), magnetic power ($\dot{W}_{\mathrm{mag}}$) and COP_{AMR}. In the present work, the performance of the AMR will be evalueted using $\dot{Q}_{\mathrm{c}}$, $\dot{W}_{\mathrm{pump}}$ and COP_{AMR}.

The cooling capacity, pumping power, magnetic power and COP_{AMR} are calculated as:

$$\dot{Q}_{\mathrm{C}} = \frac{1}{\tau}\int_{\tau_{\mathrm{HB}}} \dot{m}_{\mathrm{f}}(t) c_{\mathrm{p,f}}(T)\,(T_{\mathrm{C}} - T_{\mathrm{f,CE}})\,\mathrm{d}t \tag{8}$$

$$\dot{W}_{\mathrm{pump}} = \frac{1}{\tau}\int_0^{\tau} \frac{\dot{m}_{\mathrm{f}}(t)}{\rho_{\mathrm{f}}(T)}\Delta P\,\mathrm{d}t \tag{9}$$

$$\dot{W}_{\mathrm{mag}} = \frac{m_{\mathrm{s}}}{\tau}\oint T_{\mathrm{s}} ds \tag{10}$$

$$\mathrm{COP}_{\mathrm{AMR}} = \frac{\dot{Q}_{\mathrm{c}}}{\dot{W}_{\mathrm{pump}} + \dot{W}_{\mathrm{mag}}} \tag{11}$$

where τ is the cycle period, T_{C} is the cold end temperature, τ_{HB} is the hot blow period, $\dot{m}_{\mathrm{f}}$ is the mass flow rate, ΔP is the total pressure drop through the regenerator and s is the solid (MCM) entropy.

3. SIMULATION PARAMETERS AND PROPERTIES

In this section the geometric, porous medium, operational and fluid parameters are defined. With the exception of parameters related to the fluid properties, which are the object of the study, only the lenght of the regenerator (L_{AMR}) and mass flow rate ($\dot{m}_{\mathrm{f}}$) are varied, all the other paramaters shown are kept fixed.

3.1 AMR geometry

In the present study, the regenerator geometry consists of a rectangular prism. Table 1 summarizes the values for the height (H_{AMR}), width (W_{AMR}) and lenght (L_{AMR}). Geometry 1 was used in the first block of simulations (varying fluid properties) and Geometry 2 for the second block (different existing fluids).

Table 1: Regenerator dimensions for each geometry

Name	Dimension	Unit	Value
Geometry 1	L_{AMR}	mm	150
	H_{AMR}	mm	45
	W_{AMR}	mm	59
Geometry 2	L_{AMR}	mm	130
	H_{AMR}	mm	45
	W_{AMR}	mm	59

3.2 Porous medium (MCM) parameters

The regenerator porous medium (MCM) consists of a packed spheres bed composed of La(FeMnSi)$_{13}$H$_{\mathrm{y}}$ alloy provided by Vacuumschmelze GmbH & Co. KG. Table 2 summarizes the MCM parameters, details about each parameter can be found in (Vieira, 2020).

Table 2: Porous medium parameters

Parameter	Description	Unit	Value
d_{p}	Particle diameter	mm	0.65
N_{layers}	Number of layers	-	12
ε	Porosity	-	0.39

3.3 Operational parameters

The operational parameters, with the exception of mass flow rate ($\dot{m}_{\mathrm{f}}$), were defined based in previous results for the AMR optimal performance (Lang, 2018; Peixer, 2020; Vieira, 2020). The mass flow rate was varied from 500 kg/h to 900 kg/h in steps of 100 kg/h. Table 3 summarizes the operational parameters, more details about each parameter can be found in Vieira (2020).

Table 3: Operational parameters

Parameter	Description	Unit	Value
T_{C}	Cold end temperature	K	290.15
T_{span}	Temperature span	K	26
f_{AMR}	Frequency	Hz	2
F_{blow}	Blow fraction	-	0.375
$\dot{m}_{\mathrm{f}}$	Mass flow rate	kg/h	500 - 900

3.4 Fluid varied properties

For the first block of simulations, Geometry 1 was used and three cases were simulated. The following heat transfer fluid properties and related quantities were varied: k_{f}, ρ_{f} and h. For this purpose, water properties (k_{water}, ρ_{water}, $c_{\mathrm{p,water}}$ and μ_{water}) obtained from the *software* Engineering Equation Solver EES (Klein, 2013) were used as reference values. Table 4 summarizes the chosen variables and shows the magnitude of the variation.

Table 4: Influences studied in the first block of simulations using Geometry 1

Case	Influence studied	Unit	Value
1	Increasing density (ρ_{f})	kg/m^3	$2\rho_{\mathrm{water}}$
2	Increasing thermal conductivity (k_{f})	W/mK	$3k_{\mathrm{water}}$

For performance comparison in the results and discussions section, an AMR operating with real water properties (without the variations mentioned above) was also simulated. One shall mention that, using Case 1 as an example, while the value of density was increased 2 times, all other fluid related properties were the reference water values (see Tab. 5 for reference values).

3.5 Real fluids

For the second block of simulations, Geometry 2 was used and three diferent fluids simulated:

1. **Water/ethylene glycol 50 vol.% solution:** ehylene glycol is a common additive used in the heat transfer fluid of AMRs as it prevents the corrosion of the MCM (Kitanovski *et al.*, 2015) and lower the freezing point of the fluid (Yue *et al.*, 2012). The 50 vol.% was chosen based on automotive applications (Yue *et al.*, 2012) and aiming to achieve considerable properties variations when compared to pure water. The thermohydraulic properties were obtained from the *software* Engineering Equation Solver EES.

2. **Water with nanoparticles of aluminum oxide:** nanofluids are potential heat transfer fluids with enhanced thermohydraulic properties, they consist of a base fluid with nano-sized particles (usually metalic) suspended within them (Saidur *et al.*, 2011). After a literature review (Devendiran and Amirtham, 2016; Gupta *et al.*, 2017), water was chosen as the base fluid and aluminum oxide (Al_2O_3) as the nanoparticle due to simplicity and promising results. The nanoparticle volume fraction (ϕ) was defined as 4% and the diameter (d) as 38 nm. The thermohydraulic properties were obtained from Minea (2015).

3. **Silicone oil:** this fluid was selected as it is often used in thermal systems (Kitanovski *et al.*, 2015) and has high thermal stability, large temperature range and environmental acceptability (Jung *et al.*, 2015). The thermohydraulic properties were obtained from Kitanovski *et al.* (2015).

For reference values, Tab. 5 summarizes the thermohydraulic properties (evalueted at 20 °C) for the simulated fluids. As in the first block of simulations, an AMR operating with water was also simulated for comparison purposes.

Table 5: Reference values for the thermodydraulic properties of the fluids evaluated in the second block of simulation using Geometry 2

Fluid	$c_{\mathrm{p,f}}$ [J/kgK]	ρ_{f} [kg/m^3]	k_{f} [W/mK]	μ_{f} [Pas]
Water	4184	998	0.534	0.0010
Water/eglycol 50 vol.% solution	3364	1070	0.364	0.0043
Water + Al_2O_3 (ϕ = 4%, d = 38 nm)	3730	1198	0.686	0.0015
Silicone oil	1620	855	0.163	0.0013

4. RESULTS AND DISCUSSIONS

In this section, the results for both blocks of simulations are displayed and discussed. The results are displayed in plots of cooling capacity ($\dot{Q}_{\mathrm{c}}$), pumping power ($\dot{W}_{\mathrm{pump}}$) and coefficient of performance (COP_{AMR}) as a function of mass flow rate ($\dot{m}_{\mathrm{f}}$).

4.1 Results for the fluid varied properties

Starting with the water reference cases, Fig. 3 shows the typical influence of the mass flow rate in the cooling capacity. The cooling capacity increases with the mass flow rate until a maximum value is achieved, then the cooling capacity starts to decrease. This effect can be explained by the viscous dissipation due to the pressure drop, which starts to dominate over heat transfer in the AMR after around 800 kg/h, deteriorating its performance. For the pumping power, Fig. 4a shows the typical behavior, where the increasing mass flow rate results in increasing flow superficial velocity that causes a non-linear growth in the pressure drop and pumping power (see Eq. (1) and Eq. (8)). For the coefficient of performance, Fig. 4b also shows the typical influence of the mass flow rate in the coefficient of performance, where the peaks of cooling capacity and COP_{AMR} do not necessarily coincide as a result of the steeper increase in the pumping power as the mass flow rate increases. In summary, as the mass flow rate increases the COP_{AMR} is more sensitive to viscous losses than to the cooling capacity.

For the cases with $\rho_{\mathrm{f}} = 2\rho_{\mathrm{water}}$, Fig. 3 shows that increasing the density shifted the peak values of cooling capacity to higher mass flow rates, which can be explained by the reduced flow superficial velocity that will result in even lower values of pressure drop (see Eq. (1)), thus higher values of mass flow rate will be needed for the viscous dissipation to dominate over the heat transfer. For the pumping power, as expected from the increased density and decreased surface velocity (see Eq. (8)), Fig. 4a shows the drastic reduction in the pumping power values and less steeper shape for the cases with $2\rho_{\mathrm{water}}$. For the coefficient of performance in Fig. 4b, as similar results for cooling capacity were observed for the water reference and $2\rho_{\mathrm{water}}$ cases, the improvements in the coefficient of performance when compared to the water reference cases are due to the drastic reduction in pumping power. The COP_{AMR} showed lower sensitivity to increasing mass flow rate as the viscous losses effect was reduced.

For the cases with $k_{\mathrm{f}} = 3k_{\mathrm{water}}$, Fig. 3 shows that increasing the fluid thermal conductivity has large impacts on the cooling capacity. Furthermore, the peak values of $\dot{Q}_{\mathrm{c}}$ were also shifted to higher mass flow rates. Keeping the other parameters fixed and increasing the fluid thermal conductivity will result in a lower Prandtl number (see Eq. (6)) and consequently in a lower Nusselt number (see Eq. (7)). However, as the Nusselt number grows with $Pr^{\frac{1}{3}}$ for one of the terms in the Nusselt correlation, the increase in the fluid thermal conductivity will outweight the decrease in the Nusselt number when calculating the interstitial heat transfer coefficient (see Eq. (7)). In summary, the increase of k_{fluid} will result in higher heat transfer, which explains the gain in cooling capacity and the shift of the peak value to higher mass flow rates. In general, it has been shown that high heat transfer, while keeping the other parameters fixed, allows higher mass flow rates (Petersen, 2008). For the pumping power in Fig. 4a, as expected based on Eq. (1) and Eq. (8), the thermal conductivity has no effect in the pumping power. The values correspond to same as in the water reference cases and so were not displayed. Finally, for the coefficient of performance in Fig. 4b, as the value of pumping power is the same for the water reference and $3k_{\mathrm{water}}$ cases, the increase in the coefficient of performance is due to the higher values of cooling capacity. With increasing mass flow rate, the high sensibility of COP_{AMR} to viscous losses can once again be seen, as in the water reference cases.

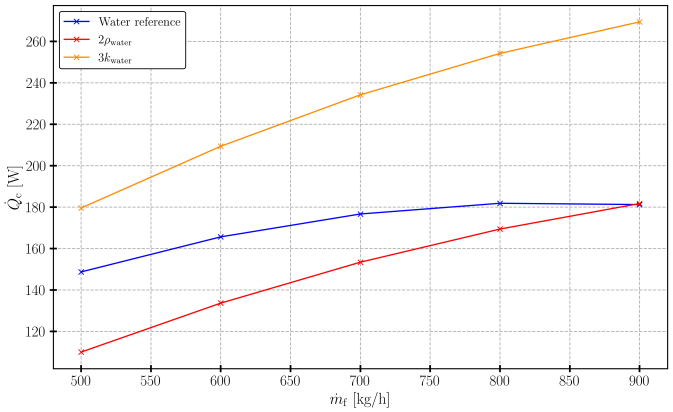

Figure 3: Cooling capacity as a function of mass flow rate for the cases with fluid varied properties.

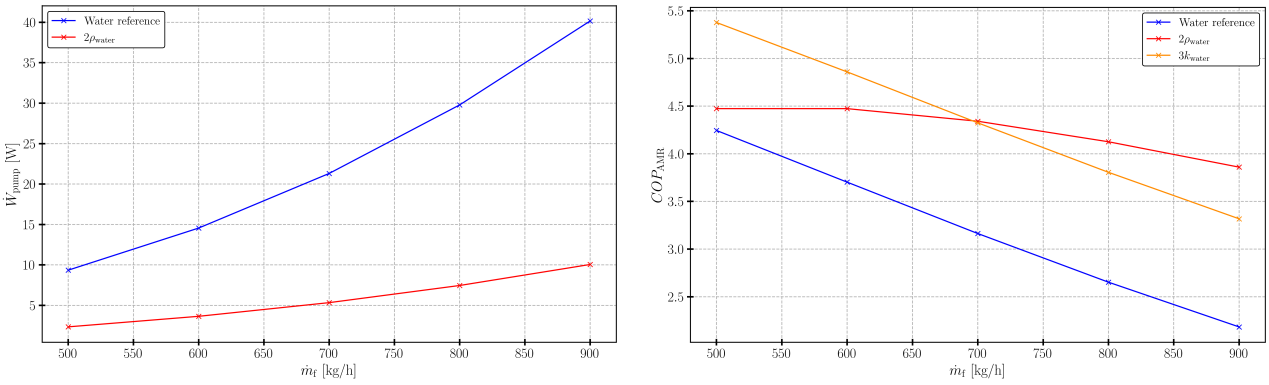

(a) (b)

Figure 4: For the cases with fluid varied properties (a) pumping power as a function of mass flow rate and (b) coefficient of performance as a function of mass flow rate.

4.2 Results for the real fluids

As the behaviour of the $\dot{Q}_c$, $\dot{W}_{\text{pump}}$ and COP_{AMR} as a function of the mass flow rate for an AMR with water as heat transfer fluid has been previous explained in the past subsection, we start with the water/ethylene glycol 50 vol.% solution, Fig. 5a shows that the 50 vol.% ethylene glycol solution presented poor performance in terms of cooling capacity when compared to pure water. Furthermore, the peak values were shifted to lower mass flow rates. Both behaviors can be explained mainly by the solution very high value of μ_f and also poor k_f, which will reduce the interstitial heat transfer coefficient (see Eq. (5), Eq. (6) and Eq. (7)). The high value of μ_f will also increase the viscous dissipation (see Eq. (1) and Eq. (2)), which will dominate over the the heat transfer. The reduction in the cooling capacity can also be understood by looking at the NTU values in Fig. 5b, which are considerably lower when compared to pure water.

For the pumping power in Fig. 6a, as one can expect based on Eq. (1) and Eq. (8), the high viscosity will cause higher pressure drops and consequently higher values of pumpimg power. Therefore, due to its higher viscosity, the water/ethylene glycol 50 vol.% solution was the fluid with the worst performance in terms of pumping power. For the coefficient of performance in Fig. 6b, as a result of the reduction in the cooling capacity and especially due to very high values of pumping power, the solution had very poor performance in terms of COP_{AMR}. In summary, in terms of performance , the 50 vol.% ethylene glycol solution suffers from poor thermal conductivity and its very high viscosity. As fluid freezing in AMRs is usually not a problem, the vol.% of this additive should be defined at the minimum value that guarantees no MCM corrosion.

For the water with nanoparticles of Al_2O_3, Fig. 5a shows a slight increase in cooling capacity when compared to pure water. Also, the peak values of $\dot{Q}_c$ were shifted to higher mass flow rates. As all the nanofluid properties differ significantly from the pure water ones, the best way to undestand is looking at the NTU in Fig. 5b, which will be significant higher for the nanofluid. This increase can be explained, as also discussed in previous subsection, due to the increase in the thermal conductivity. For the pumping power, Fig. 6a shows no significant changes in pumping power were observed when compared to pure water. This behavior can be explained as a balance between the effect of the density and the viscosity. The nanofluid presents higher values of ρ_f and μ_f when compared to pure water, the first tends to reduce the pumping power and the second tends to increase it.

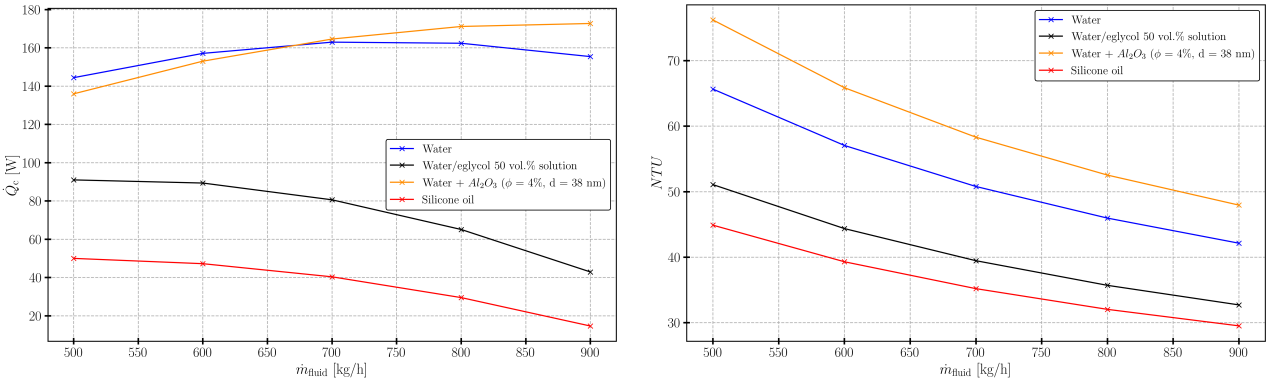

(a) (b)

Figure 5: For the cases with real fluids (a) cooling capacity as a function mass flow rate and (b) NTU as a function mass flow rate.

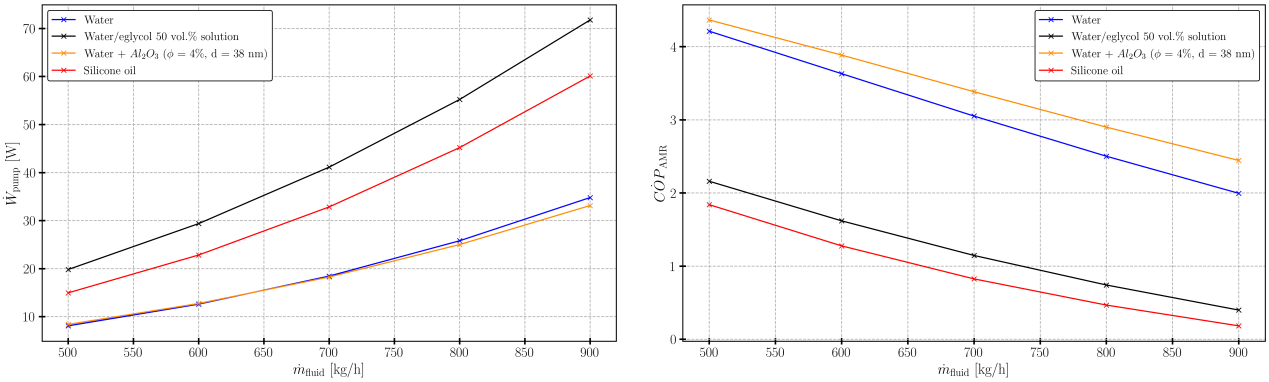

(a) (b)

Figure 6: For the cases with real fluids (a) pumping power as a function of mass flow rate and (b) coefficient of performance as a function of mass flow rate.

For the coefficient of performance in Fig. 6b, one variable that was not shown in this study is the magnetic work ($\dot{W}_{\mathrm{mag}}$), which was slight lower for the nanofluid. This explains why the coefficient of performance was higher than the pure water ones for low mass flow rates. As the mass flow rate increases, the higher values of COP_{AMR} when compared to pure water are explained by the increase in the cooling capacity. In summary, in terms of performance, water with nanoparticles of Al_2O_3 showed promising results, as it benefits from its enhanced thermal conductivity caused by the addition of the metallic nanoparticle.

Finally, for the silicone oil, Fig. 5a shows that the silicone oil presented very poor performance in terms of cooling capacity when compared to pure water. Also, the peak values were shifted to lower mass flow rates. This behaviors can be explained by looking at the NTU in Fig. 5b, which will be the lowest for the silicone oil. As this fluid has the lowest values of $c_{\mathrm{p,f}}$, this NTU reduction is only explained by a big reduction in the interstitial heat transfer coefficient (see Eq. (4)). This decrease can be explained, as already discussed extensively, by the fluid thermal conductivity, which for the silicone oil is the lowest. For the pumping power in Fig. 6a, as one can expect based on Eq. (1) and Eq. (8), the higher value of viscosity and the lower value of density when compared to pure water will cause higher pressure drops and consequently poor performance in terms of pumping power.

For the coefficient of performance in Fig. 6b, as a consequence of very poor performance in terms of cooling power and high values of pumping power, the silicone oil presented the lowest COP_{AMR} of all evaluated fluids. In summary, in terms of performance, the silicone oil suffers from very low thermal conductivity, higher viscosity and lower density when compared to pure water. As AMRs usually operate at close to ambient temperatures and small temperature spans, there is no necessity of fluids with large working temperature ranges (as silicone oil).

5. CONCLUSIONS

In terms of performance improvement of an AMR, studies usually focus on the magnetocaloric material, regenerator geometry, magnetic field and operating parameters such as mass flow rate, frequency, blow fraction, cold end temperature and temperature span. In other words, the influence of the heat transfer fluid is usually left out or superficially analyzed. In

this study, the effect of the heat transfer fluid in the performance an AMR was evaluated with an experimentally validated one-dimensional AMR model.

In the first part, the effect of the fluid thermal conductivity was analyzed in a isolated way and found to have impressive impacts in terms of cooling capacity, increasing the heat transfer phenomenon. The analysis was repeated for the fluid density and found the former to have great impacts in the pumping power and also in reducing the viscous losses dominance with the increasing mass flow rate. Evidently, enhancing the fluid properties in an isolated way its not possible in real applications as there will always be a trade-off between them. The cases were simulated to show how the selected properties impact the AMR performance and to provide guidelines for possible AMR heat transfer fluid selections, enhancements and future studies. In real applications, this kind of improvement depends on how much these properties can actually be improved.

In the second part, aiming at real applications, the performance of the AMR with diffent real fluids was evaluated. The results were analyzed and it was noticed that adding metallic nanoparticles to the baseline water (creating a nanofluid) showed improved and promising results in terms of cooling capacity and coefficient of performance. One shall highlight that nanofluids are a relatively new class of fluids (Saidur *et al.*, 2011) which has shown promising results and have been an area of great research, however, few barriers and challenges still exist in this area (Gupta *et al.*, 2017). Nevertheless, from the results, the addition of nanoparticles or additives to enhance the thermohydraulic properties of the heat transfer fluid was found to be a promising point for performance improvements and future studies

6. ACKNOWLEDGEMENTS

Financial support from CNPq, CAPES, CODEMGE and the EMBRAPII Unit Polo/UFSC is duly acknowledged

7. REFERENCES

Bansal, P., E, V. and O, A., 2012. "Status of not-in-kind refrigeration technologies for household space conditioning, water heating and food refrigeration". *International Journal of Built Environment and Sustainability*, Vol. 1, pp. 85–101.

Barclay, J.A. and Steyert, W.A., 1982. "Active magnetic regenerator".

Devendiran, D.K. and Amirtham, V.A., 2016. "A review on preparation, characterization, properties and applications of nanofluids". *Renewable and Sustainable Energy Reviews*, Vol. 60, pp. 21–40.

Ergun, S., 1952. "Fluid flow through packed columns". *Chem. Process Eng. London*, Vol. 48, pp. 89–94.

Fortkamp, F.P., 2019. *Integrated Design of the Magnet-Regenerator assembly for a magnetic refrigerator*. Ph.D. thesis, Federal University of Santa Catarina, Florianópolis, Brasil.

Gupta, M., Singh, V., Kumar, R. and Said, Z., 2017. "A review on thermophysical properties of nanofluids and heat transfer applications". *Renewable and Sustainable Energy Reviews*, Vol. 74, pp. 638–670.

Jung, C., Dersch, J., Nietsch, A. and Senholdt, M., 2015. "Technological perspectives of silicone heat transfer fluids for concentrated solar power". *International Conference on Concentrating Solar Power and Chemical Energy Systems, SolarPACES*, Vol. 69, pp. 663–671.

Kaviany, M., 1995. *Principles of Heat Transfer in Porous Media*. Springer, 2nd edition.

Kitanovski, A., Tušek, J., Tomc, U., Plaznik, U., Ožbolt, M. and Poredoš, A., 2015. *Magnetocaloric Energy Conversion: From Theory to Applications*. Springer.

Klein, S.A., 2013. "Engineering equation solver (ees) professional version". *V9.339, F-Chart Software, Madison, WI.*

Lang, G.B., 2018. "Development of an active magnetic regenerator model using the finite volumes method for a magnetic refrigeration application".

Minea, A.A., 2015. "A study on brinkman number variation on water based nanofluid heat transfer in partially heated tubes". *KONA Powder and Particle*, Vol. 32.

Monfared, B., 2018. "Design and optimization of regenerators of a rotary magnetic refrigeration device using a detailed simulation model". *International Journal of Refrigeration*, Vol. 88, pp. 260–274.

Pallares, J. and Grau, F.X., 2010. "A modification of a nusselt number correlation for forced convection in porous media". *International Communications in Heat and Mass Transfer*, Vol. 37, pp. 1187–1190.

Peixer, G.F., 2020. *Integrated Design and Optimization of a Magnetic Cooling System for Air-Conditioning Applications*. Master's thesis, Federal University of Santa Catarina, Florianópolis, Brasil.

Petersen, T.F., 2008. *Numerical modelling and analysis of a room temperature magnetic refrigeration system*. Ph.D. thesis, Federal University of Santa Catarina, Danmarks Tekniske Universitet, Risø Nationallaboratoriet for Bæredygtig Energi.

Rowe, A., Tura, A., Dikeos, J. and Chanine, R., 2005. "Near room temperature magnetic refrgeration". In *Proceedings of the International Green Energy Conference*.

Saidur, R., Leong, K.Y. and Mohammed, H.A., 2011. "A review on applications and challenges of nanofluids". *Renewable and Sustainable Energy Reviews*, Vol. 15, pp. 1646–1668.

Trevizoli, P.V., 2015. *Development of thermal tegenerators for magnetic cooling applications.* Ph.D. thesis, Federal

University of Santa Catarina, Florianópolis, Brasil.

Trevizoli, P.V., Nakashima, A.T. and Barbosa Jr, J.R., 2016. "Performance evaluation of an active magnetic regenerator for cooling applications - part ii: mathematical modeling and thermal losses". *International Journal of Refrigeration*, Vol. 72, pp. 206–217.

Vieira, B.P., 2020. *Modeling and optimization of active magnetic regenerators using La-Fe-Si based alloys*. Master's thesis, Federal University of Santa Catarina, Florianópolis, Brasil.

Yue, H., Zhao, Y., Ma, X. and Gong, J., 2012. "Ethylene glycol: properties, synthesis, and applications". *Chemical Society Reviews*, Vol. 41, p. 4089–4380.

8. RESPONSIBILITY NOTICE

The authors are solely responsible for the printed material included in this paper.